Validating Drag and Heating Coefficients for Hollow Reentry Objects in Continuum Flow Using a Mach 7 Ludwieg Tube

Chris Ostrom[(1)], Jeremiah Marichalar[(2)], Benton Greene[(3)], Angelina Andrade[(4)], Eugene N.A. Hoffman[(4)], Elijah J. Lalonde[(4)], Christopher S. Combs[(4)]

[(1)] NASA Johnson Space Center, Mail Code XI5-9E, 2101 NASA Parkway, Houston, TX 77058
[(2)] GeoControl Systems – Jacobs JETS II ContractNASA Johnson Space Center, Mail Code JE07A, 2101 NASA Parkway, Houston, TX 77058
[(3)] Jacobs, NASA Johnson Space Center, Mail Code XI5-9E, 2101 NASA Parkway, Houston, TX 77058
[(4)] Department of Mechanical Engineering, University of Texas at San Antonio, San Antonio, TX 79249

ABSTRACT

Drag and heating coefficient databases and models are crucial to destructive reentry simulation. The NASA Orbital Debris Program Office (ODPO) develops, maintains, and performs analysis with the Object Reentry Survival Analysis Tool (ORSAT), which comprises drag and heating models for free molecular, transitional, and continuum flow regimes. These models have, in the past, only included solid, convex, blunt shapes (such as boxes, spheres, and cylinders). Previous work led by ODPO includes the extension of these models to hollow cylinders and square boxes in free molecular and transitional flow using the Direct Simulation Monte Carlo (DSMC) method.

Since 2019, the ODPO has continued its program of DSMC simulations and extended the project to include analyses with the NASA Data Parallel Line Relaxation (DPLR) program on hollow cylinders and boxes (with varying wall thickness-diameter ratio). In fall 2022, the ODPO began a collaboration with the University of Texas San Antonio (UTSA) to use the Mach 7 Ludwieg Tube facility to validate the model built using numerical simulations. This facility can replicate (at a scale of approximately 100:1) the conditions seen by reentering objects near typical demise altitudes. We present here the drag and heating coefficients derived from the continued DSMC simulations, the new DPLR simulations, and the 26-test series at UTSA.

1 Introduction

The Object Reentry Survival Analysis Tool (ORSAT), version 7.0, implemented a simple model for drag and aeroheating for hollow objects in rarefied and transitional flow with the results of a series of Direct Simulation Monte Carlo (DSMC) gas dynamic simulations using the NASA DSMC Analysis Code (DAC) [1]. A total of 162 cases were simulated, using both right circular cylinders and square prisms at a single flow condition, but varying inner diameter, length, angle of attack, and Knudsen number (by varying the outer diameter). The results of these simulations (integrated drag force and heating rate) were normalized by the appropriate area for different tumbling modes and added as the 21st-27th shape primitives for ORSAT analysis using simple table lookups and multidimensional interpolation.

The goal of this project is to provide, first, a better criterion for estimating when an object should be "unrolled" (*e.g.*, breaking a ring into a cylinder or a tube into a flat plate); and second, to improve the estimation of drag and heating for those objects that cannot be treated as either a solid object with the same outer dimensions as the hollow object, or be unrolled. For this second phase of the hollow object characterization project, 1000 further simulations were conducted using DAC, with simulation parameters as in Table 1 (the parameters from phase 1 are also reproduced here from [1]). One of the main differences with the second phase of DAC simulations is that the runs were conducted at multiple altitudes along a reentry trajectory (hence freestream density varies), but the outer diameter of the object remains constant. A more detailed discussion of these DAC simulations will be given in Section 2.

In late 2022, the Orbital Debris Program Office (ODPO) conducted a test series at the University of Texas San Antonio (UTSA) Mach 7 Ludwieg Tube facility [2]. During this test series, 27 tests were conducted, with 24 using free-flying cylinder and square prism models to estimate drag force and moments, and three tests with strut-mounted cylinder models to optimize the measurement of heat fluxes on the ram face. In addition to the two shape parameters, the inner diameters (*i.e.*, hole sizes) and lengths were varied for the models to provide validation data

for future gas dynamic simulations for low-speed flows. Table 2, reproduced from [2], shows the shape parameters used for the 25 drop tests.

Table 1. DSMC Simulation Conditions for Phase 1 and Phase 2 of Hollow Body Characterization Project.

Quantity	Phase 1 Values	Phase 2 Values
Altitude (km)	111.375	97.3 – 128.4
Freestream Speed (m/s)	7800	7800
Freestream Density (kg/m3)	7.61E-8	7.61E-7 to 7.6E-9
Freestream Temperature (K)	265	265
Wall Temperature (K)	300	300
Knudsen Number ()	0.2, 1, 10	0.1, 0.5, 1, 5, 10
Outer Diameter (m)	0.1, 1, 5	1
ID/OD Ratio ()	0.1, 0.5, 0.95	0.1, 0.5, 0.95
Angle of Attack (°)	0, 45, 90	0, 22.5, 45, 67.5, 90
L/D Ratio ()	0.1, 0.5, 1.0	0.1, 0.5, 1, 2, 5

Table 2. List of geometric variables for wind tunnel test series.

Cross Section	Diameter or Width (inches)	Length (inches)	Inner Hole Size (inches)
Circle	0.5	0.125	0 (Solid)
Circle	0.5	0.125	1/16
Circle	0.5	0.125	1/4
Circle	0.5	0.125	3/8
Circle	0.5	0.5	0 (Solid)
Circle	0.5	0.5	1/16
Circle	0.5	0.5	1/4
Circle	0.5	0.5	3/8
Circle	0.5	1.5	0 (Solid)
Circle	0.5	1.5	1/16
Circle	0.5	1.5	1/4
Circle	0.5	1.5	3/8
Square	0.5	0.125	0 (Solid)
Square	0.5	0.125	1/16
Square	0.5	0.125	1/4
Square	0.5	0.125	3/8
Square	0.5	0.5	0 (Solid)
Square	0.5	0.5	1/16
Square	0.5	0.5	1/4
Square	0.5	0.5	3/8
Square	0.5	1.5	0 (Solid)
Square	0.5	1.5	1/16
Square	0.5	1.5	1/4
Square	0.5	1.5	3/8

The 24 drop tests were conducted using UTSA's typical configuration, with the Ludwieg tube's driver section filled with pressurized air (in our tests, around 85-105 psi when the diaphragms burst), heated to approximately 700K, the limit for the tunnel. Two of the final three tests that utilized the sting arm to firmly mount the cylindrical models were run using pressurized helium, allowing the test section Mach number to reach 11.0, extending the capability of the UTSA facility without hardware changes, and allowing for collection of validation data further into the region of interest for reentry demisability.

2 Direct Simulation Monte Carlo (DSMC) Simulations

The DSMC simulations conducted for phase 2 of the hollow body characterization project used largely the same approach as that followed in the authors' previous paper. [1] For the 2 shapes under consideration (right circular cylinders and square prisms), 15 unique geometries were constructed, using the fineness ratio (length-to-diameter ratio, L/D) and inner-diameter-to-outer-diameter ratio (ID/OD). The Knudsen number was varied for the simulations by changing the freestream density. The angle of attack, defined as α in Fig. 1, reproduced from [1], was also varied from 0-90 degrees, in increments of 22.5 degrees, to improve the estimates for tumbling heating and drag coefficients from phase 1.

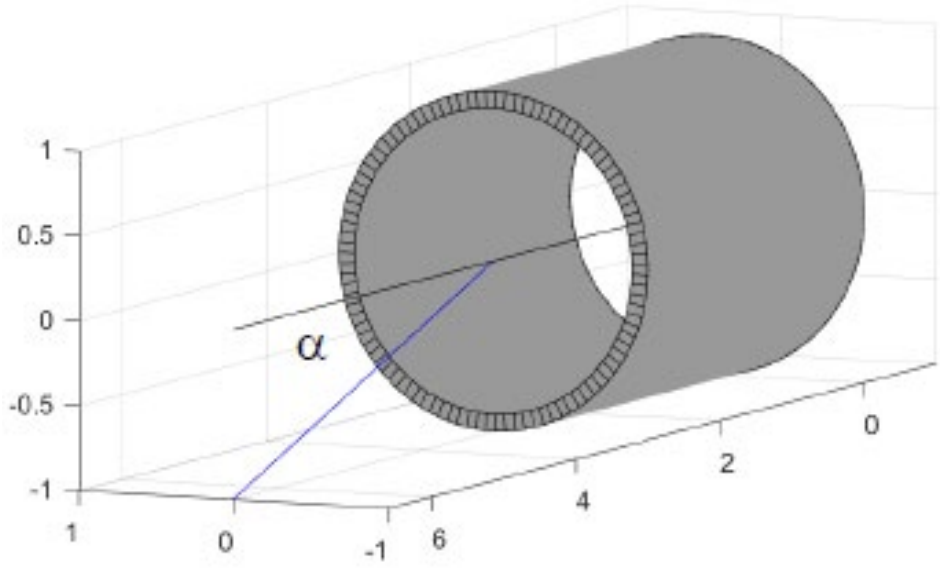

Fig. 1. Angle of attack definition.

Since the full case matrix consists of 1000 simulations, only a brief set of plots will be included here to show the general behavior of the flow field around hollow objects flying at a zero angle of attack. Figure 2 includes a series of square prisms with an ID/OD of 0.95 and varying L/D (again, from 0.1 to 5) at a Knudsen number of 0.1. It is clear that the object allows for flow through the hole for low L/D, but even at an L/D of 0.5, it appears that flow through the object may be choked, contributing to significant drag. As the L/D continues to increase all the way to 5, the "bubble" of near- or sub-sonic flow also grows past the aft end of the body. Figure 3 shows the same geometry, but at an angle of attack of 22.5 degrees. The trend of increasing near- or sub-sonic flow bubble size seen in Fig. 2 is still apparent, but the non-zero angle of attack causes massive flow disruption for objects with higher L/D.

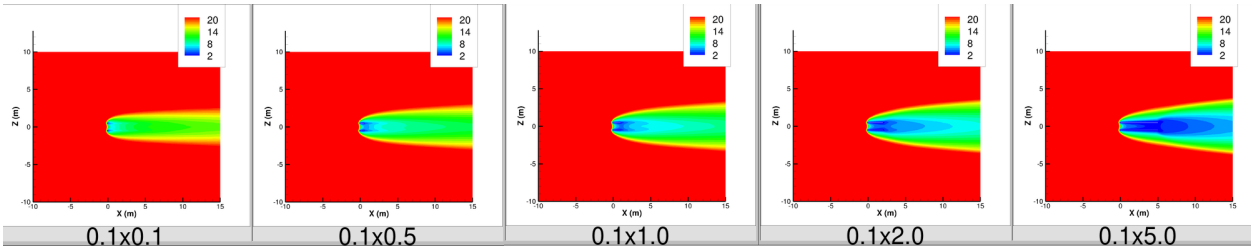

Fig. 2. Series of contour plots of Mach number for a DAC simulation of a square prism of ID/OD 0.95 at a Knudsen number of 0.1 and angle of attack of 0 degrees, with varying L/D.

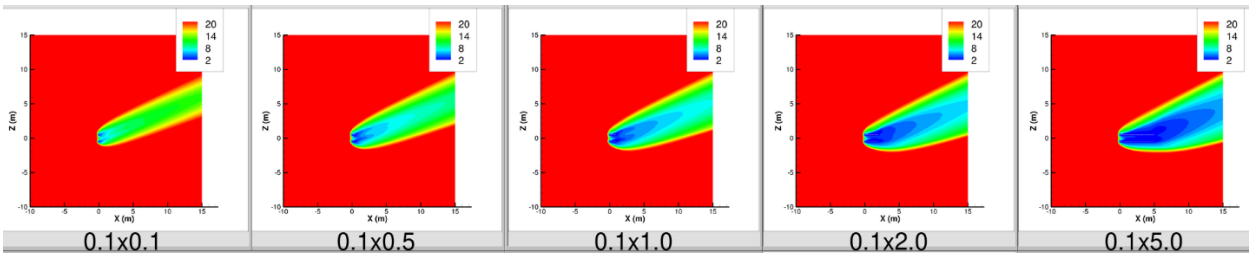

Fig. 3. Series of contour plots of Mach number for a DAC simulation of a square prism of ID/OD 0.95 at a Knudsen number of 0.1 and angle of attack of 22.5 degrees, with varying L/D.

Once the drag force is extracted for each simulation case, the results can be averaged for a single geometry and flow condition across the five angles of attack to produce a tumbling-average drag or heating coefficient. Based on the assumed attitude motion, three models can be produced for the square prisms (two fixed attitudes, ram-facing and broadside, and one end-over-end tumbling mode) and four models for the circular cylinders (the same three as the square prism, plus a broadside spinning mode). Figure 4 shows a comparison of the drag coefficients for solid, ID/OD = 0.5, and ID/OD = 0.95 DAC-derived models and compares against the ORSAT model for solid cylinders, scaled to an equivalent drag area (and using L/D = 0.5). Note that for easier comparison between hollow objects, we have normalized by the full area of the ram-facing surface (*i.e.*, the area for normalization of the drag coefficient includes the area of the hole).

In all cases, the drag predicted by ORSAT's solid object model is lower than the DAC-derived drag coefficients, though the errors are typically only of order 10-20% for the cases where ID/OD is less than 0.5. The areas of most concern (*i.e.*, largest differences in the models) are exactly where they were previously identified: where Knudsen number is near the lower edge of the transition regime (~0.1) and the flow through the object is close to sonic speeds (choked). The error in the ID/OD = 0.95 case grows to nearly 200% at the lowest Knudsen numbers, which is also a good check on the typical engineering analysis procedure of unrolling hollow objects. Figure 5 presents a similar comparison as Fig. 4, but with cylinders at an angle of attack of 0 degrees. Conversely, the DAC-derived drag coefficients were much lower than the default ORSAT solid object model would predict, on average 45% lower for the solid case, 20% lower for ID/OD of 0.5, and 40% higher for the ID/OD 0.95 case.

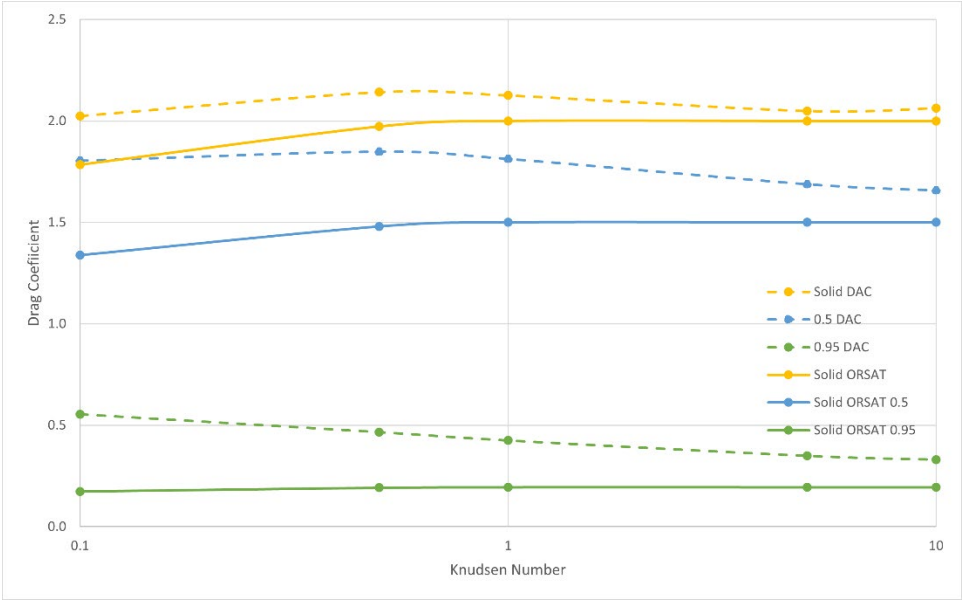

Fig. 4. Comparison of DAC-derived drag coefficients and default ORSAT model for square prism of L/D 0.5, varying ID/OD, and varying Knudsen number at zero angle of attack.

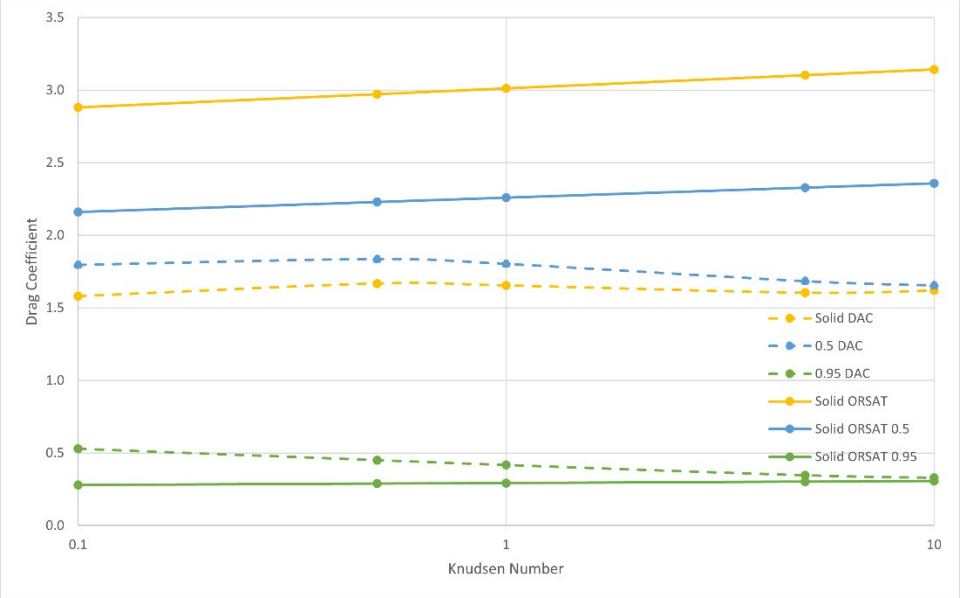

Fig. 5. Comparison of DAC-derived drag coefficients and default ORSAT model for cylinders of L/D 0.5, varying ID/OD, and varying Knudsen number at zero angle of attack.

3 University of Texas at San Antonio Hypersonics Lab

3.1 *UTSA Hypersonic Ludwieg Tube*

The UTSA Hypersonic Ludwieg tube depicted in Fig. 6, has a constant test section cross-section of 203 mm × 203 mm (8" × 8"). The driver tube can be pressurized using either compressed gas bottles or a four-stage compressor – depending on the desired gas composition – providing stagnation pressures up to approximately 14 MPa. While the primary test gas was air for this study, it is possible to test with nitrogen or other more exotic test gases depending on the needs of a given experimental campaign. Two test runs in the present effort employed helium as the test gas. With an 18-m-long folded driver tube, individual test runs have a steady-state duration of roughly 50-100 ms depending on initial conditions. The insulated driver tube pipe can be pre-heated up to 700 K for wind tunnel tests. The freestream velocity is on average 1130 m/s, resulting in freestream Reynolds numbers between 0.5-200 × 10^6 m^{-1}, making the UTSA facility one of the few at a U.S. university capable of accessing this Reynolds and Mach number range. The flow is exhausted into a roughly 6 m^3 vacuum dump tank, enabling multiple steady state passes of hypersonic flow for total test times up to 500 ms. Optical access for potential experiments can be provided by modular glass windows on the wind tunnel sidewalls, floor, and ceiling. While the facility run duration is relatively short compared to blowdown facilities, the steady test time correlates to over 1500 flow lengths for an appropriately scaled test model. It should be noted that this is a low-enthalpy hypersonic facility that can provide valuable aerothermodynamic data but does not produce background luminescence that could interfere with optical measurements. For each test run, baseline facility data were recorded using a National Instruments Data Acquisition (NI DAQ) system. Facility data include calibrated test section static pressure, plenum stagnation pressure, driver tube (burst) pressure, driver tube temperature, and camera timing/synchronization signals. A complete characterization of the facility's flow properties is found in[3].

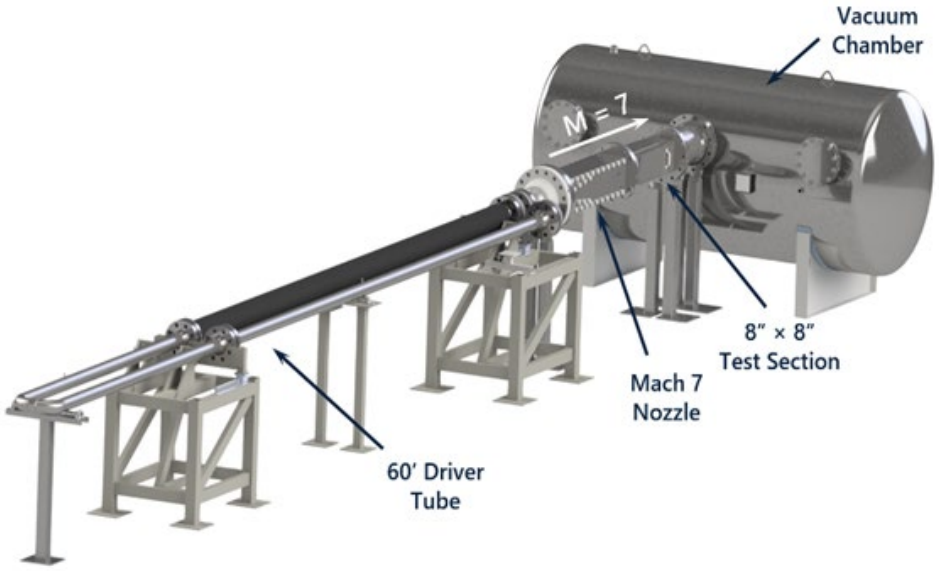

Fig. 6. Schematic of the UTSA Mach 7 Ludwieg Tube.

3.2 Experimental Setup

In this work, a quantitative high-speed imaging system permitted time-resolved object position, velocity, acceleration, pitch, and aerodynamic moment/coefficient measurements. A high-powered LED (Luminus Devices CBT-140) provided high-intensity illumination at the selected acquisition rate. The measurements were extracted from the images obtained from the high-speed camera using an in-house Python code. A total of four high-speed Photron SA-Z cameras were used to collect images for each model as seen in Fig. 7. Two of the four high-speed cameras were placed orthogonal to the tunnel in different planes to resolve motions in all three dimensions. A third camera was placed at an oblique angle at the same height as the tunnel to provide another reference point. Finally, an oblique camera from the top viewing the model head on was used to verify heating occurring on the front surface of the model where the flow was impinging. A hinge release mechanism was employed for the entirety of the test campaign. An image showing the release mechanism is provided on the left-hand side of Fig. 7. This mechanism was made from a thin piece of aluminum mounted to a hinge which collapsed and folded into a cavity on the facility's test section floor after contact with the startup flow of the tunnel. Schlieren imaging was performed to ensure this release mechanism did not have any effects on the model during free flight.

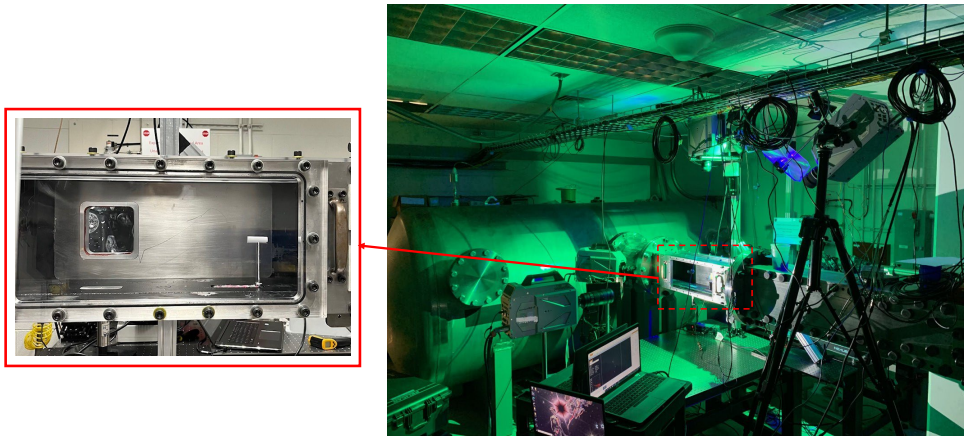

Fig. 7. Image of the four-camera setup showing various placements to achieve the desired views.

3.3 Results

Table 3 represents hypersonic testing of 27 test articles and the facility's flow conditions. A combination of high-speed imaging, temperature sensitive paint (TSP), pressure sensitive paint (PSP), and infrared (IR) imaging was performed on the given test articles to gain the required aerodynamic information. To improve the heat transfer to the models and measure temperature changes, the nominal operating stagnation temperature was increased to 700 K beginning with Test #8.

Table 3. Test Matrix

Test Number	Cross Section	Test Gas	Mach Number	T_0 (K)	P_0 (psia)	P (psia)	Re (m^{-1})
1	Circle	Air	7.2	318	92	0.042	7.82e+06
2	Circle	Air	7.2	320	93	0.042	7.81e+06
3	Circle	Air	7.2	318	92	0.039	7.84e+06
4	Circle	Air	7.2	316	98	0.040	8.39e+06
5	Circle	Air	7.2	313	90	0.044	7.83e+06
6	Circle	Air	7.2	319	86	0.034	7.27e+06
7	Circle	Air	7.2	320	106	0.039	8.90e+06
8	Circle	Air	7.2	633	105	0.037	2.69e+06
9	Circle	Air	7.2	659	81	0.033	1.94e+06
10	Circle	Air	7.2	688	355	0.085	7.98e+06
11	Circle	Air	7.2	719	92	0.038	1.91e+06
12	Circle	Air	7.2	715	215	0.096	4.52e+06
13	Square	Air	7.2	685	135	0.068	3.05e+06
14	Square	Air	7.2	708	106	0.037	2.26e+06
15	Square	Air	7.2	713	100	0.035	2.11e+06
16	Square	Air	7.2	715	102	0.040	2.14e+06
17	Square	Air	7.2	648	105	0.038	2.61e+06
18	Square	Air	7.2	684	86	0.035	1.95e+06
19	Square	Air	7.2	693	75	0.030	1.67e+06
20	Square	Air	7.2	701	84	0.032	1.84e+06
21	Square	Air	7.2	708	87	0.034	1.86e+06
22	Square	Air	7.2	714	94	0.034	1.99e+06
23	Square	Air	7.2	680	92	0.037	2.11e+06
24	Square	Air	7.2	709	89	0.035	1.91e+06
25	Circle	Helium	11.03	691	87	0.008	5.31e+06
26	Circle	Air	7.2	697	86	0.03	2.30e+06
27	Circle	Helium	11.03	722	91	0.008	5.10e+06

Figure 8 shows a sample montage from the oblique camera from Test #5. While the oblique camera was not used explicitly in the tracking algorithm, this camera was used to determine if any of the models were rolling during flight, particularly the square models. The large bright feature on the left side of the images is the interior wall of the test section of the wind tunnel, and part of the window.

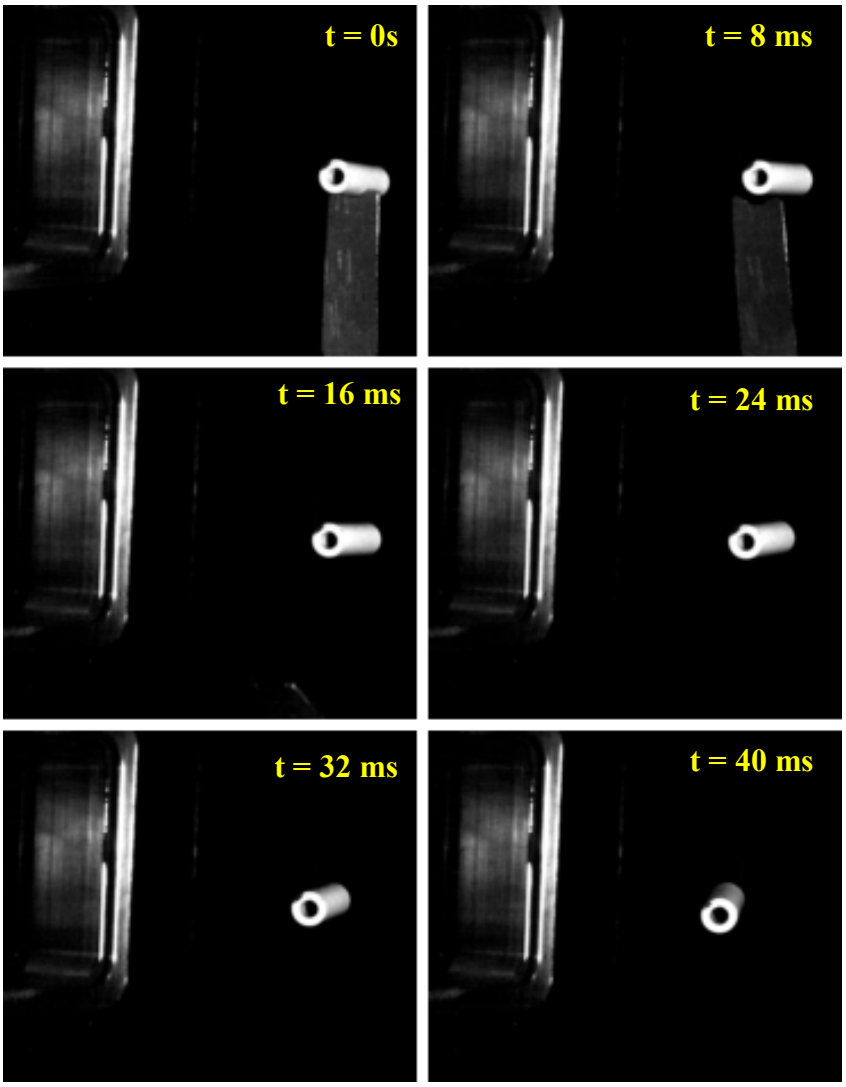

Fig, 8. Montage from a sample test showing release mechanism and model motion.

Images from the camera located normal to the test section in Fig. 7 and from the camera mounted above the wind tunnel were used in the Python object tracking code. The algorithm performs principal component analysis (PCA) on the images to determine the geometric center of the model in the image and the angular orientation. For the test articles used in the present tests, the center of mass is located at the centroid of the binary silhouette, so no transformation matrix is required to get the coordinates of the center of mass from the centroid coordinates. An example from Test #1 of the PCA output is shown in Fig. 9. The UTSA object tracking code outputs images as seen in Fig, 9 while running so that any false detections can quickly be detected and corrected. Once the PCA was done for both the normal and upper camera images, a 3D trajectory was reconstructed and the coefficient of drag for every model was found. Curve fits were applied to the object tracking results to eliminate jitter in the object tracking and prevent the subsequent propagation of the jitter in the velocity and acceleration data. Figure 10 demonstrates a sample plot of the tracked center of mass for Test #1. The black lines correspond to a second order polynomial curve fit that was applied to the data after tracking was complete.

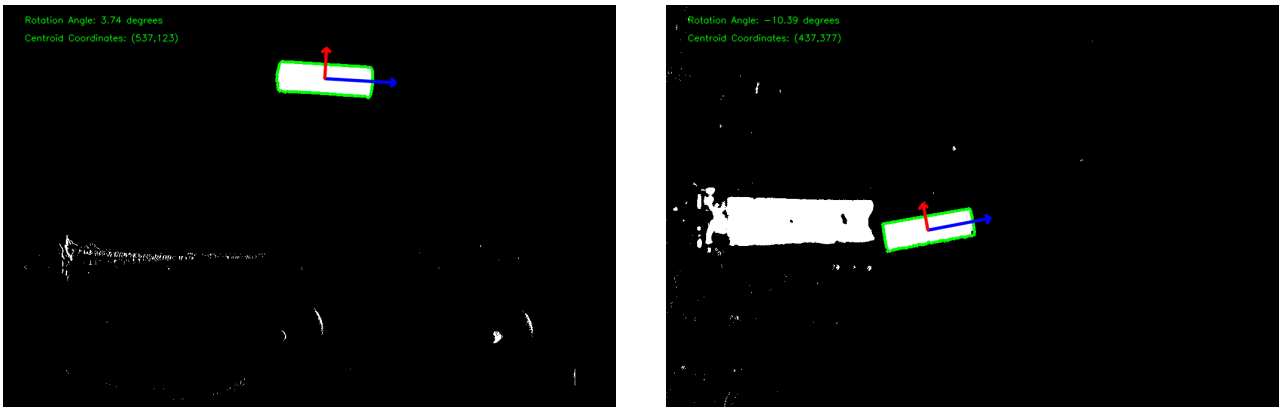

Fig. 9. Binary image from PCA tracking algorithm for the normal camera (left) and upper camera (right).

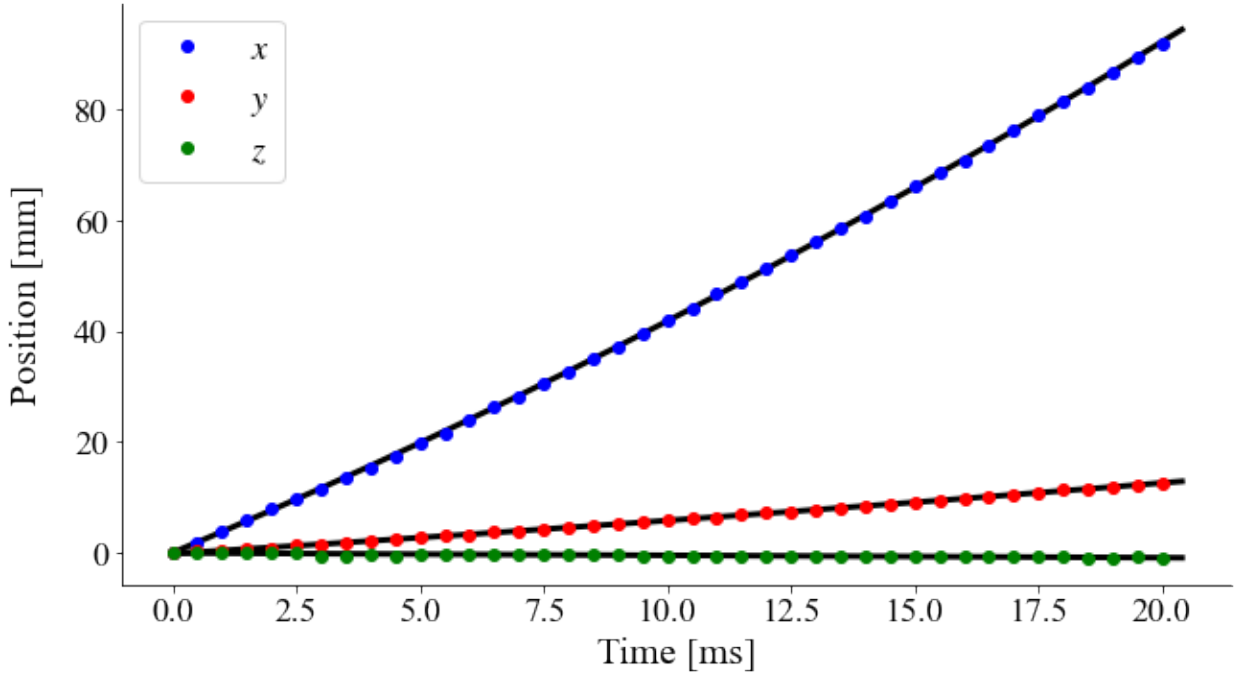

Fig. 10. Center of mass tracking from Test #1.

It is important to note that some of the test models were unable to be tracked due to background reflections in the images interfering with the object tracking algorithm. Table 4 provides the drag coefficients and moments of inertia for the models that were tracked. Aerodynamic coefficients orthogonal to the flow direction have been excluded from the table as they were nearly zero, as expected.

Table 4. Drag coefficients and moments of inertia obtained from the data analyzed.

Test Number	Cross Section	Mass (kg)	I_x (kg×m^2)	I_z (kg×m^2)	C_D
1	Circle	0.0133	2.720e-07	6.510e-06	0.0141
2	Circle	0.0130	2.706e-07	6.323e-06	0.0126
3	Circle	0.0058	1.851e-07	3.265e-06	0.0185
4	Circle	0.0009	2.224e-08	1.361e-07	0.0110
6	Circle	0.0044	9.118e-08	7.353e-07	0.0113
7	Circle	0.0034	8.465e-08	6.484e-07	0.0120
8	Circle	0.0019	6.068e-08	4.452e-07	0.0258
9	Circle	0.0011	2.267e-08	1.389e-07	0.0093
11	Circle	0.0005	1.525e-08	9.274e-08	0.0111
12	Circle	0.0049	9.967e-08	8.498e-07	0.0109
18	Square	0.0020	6.496e-08	7.139e-08	0.0130
19	Square	0.0026	7.435e-08	7.503e-08	0.0111
20	Square	0.0026	7.524e-08	7.597e-08	0.0099
21	Square	0.0038	5.599e-07	1.681e-07	0.0310
24	Square	0.0076	1.037e-06	2.172e-07	0.0127

4 Conclusions and Future Work

Additional DSMC simulations of simple hollow body shapes (cylinders and square rectangular prisms) were performed with the NASA DAC software at various angles of attack, wall thicknesses, and Knudsen number within the transitional regime, then drag and heating coefficients for each simulation were computed. Significant differences in drag coefficient were seen when comparing the built-in ORSAT models for boxes and cylinders with the recent DAC simulation results across the transitional regime, with errors of up to 50% for cylinders with ID/OD of 0.5. Square prisms were much better modeled than cylinders, with typical errors of 20% or less when comparing the previous ORSAT model with the DAC simulation results. All 1000 DAC simulations have been incorporated into a database and compiled into ORSAT 7.0, allowing analysts to select six new shape primitives: hollow box and cylinder, with tumbling, spinning, and fixed-attitude dynamic modes.

At the time of writing, simulations were in progress to compare against the wind tunnel tests conducted at UTSA, but insufficient results were available to validate those models and are not presented here. Future work will include these continuum fluid dynamic simulations to extend the aerothermodynamic database for direct use in ORSAT, as well as a new analytical model to determine hollowness automatically without analyst input.

5 References

1. Marichalar, J. and Ostrom, C., "Estimating Drag and Heating Coefficients for Hollow Reentry Objects in Transitional Flow Using DSMC," International Orbital Debris Conference, 2019. Sugar Land, Texas.
2. Ostrom, C., *et al*. "Recent Activities in Modeling Hollow Objects During Reentry," Orbital Debris Quarterly News, Vol. 27 No. 2, June 2023.
3. Hoffman, E. N., *et al*. "Flow Characterization of the UTSA Hypersonic Ludwieg Tube," *Aerospace* Vol. 10, No. 5, 2023, p. 463.